

## Positrons from particle dark-matter annihilation in the Galactic halo: propagation Green's functions

Igor V. Moskalenko<sup>§</sup> and Andrew W. Strong

*Max-Planck-Institut für extraterrestrische Physik, Postfach 1603, D-85740 Garching, Germany*

*E-mails: imos@mpe.mpg.de, aws@mpe.mpg.de*

We have made a calculation of the propagation of positrons from dark-matter particle annihilation in the Galactic halo in different models of the dark matter halo distribution using our 3D code, and present fits to our numerical propagation Green's functions. We show that the Green's functions are not very sensitive to the dark matter distribution for the same local dark matter energy density. We compare our predictions with computed cosmic ray positron spectra ("background") for the "conventional" CR nucleon spectrum which matches the local measurements, and a modified spectrum which respects the limits imposed by measurements of diffuse Galactic  $\gamma$ -rays, antiprotons, and positrons. We conclude that significant detection of a dark matter signal requires favourable conditions and precise measurements unless the dark matter is clumpy which would produce a stronger signal. Although our conclusion qualitatively agrees with that of previous authors, it is based on a more realistic model of particle propagation and thus reduces the scope for future speculations. Reliable background evaluation requires new accurate positron measurements and further developments in modelling production and propagation of cosmic ray species in the Galaxy.

95.35.+d, 98.35.Gi, 98.38.Am, 98.70.Sa

### I. INTRODUCTION

Investigations of galaxy rotation, big-bang nucleosynthesis, and large-scale structure formation imply that a significant amount of the mass of the universe consists of non-luminous dark matter [1]. Among the favored particle dark matter candidates are so-called weakly interacting massive particles (WIMPs), whose existence follows from supersymmetric models (see Ref. [2] for a review). If stable, such particles could have a significant cosmological abundance at the present time. A pair of stable WIMPs can annihilate into known particles and antiparticles and it may be possible to detect WIMPs in the Galactic halo by the products of their annihilations. The difficulty, however, consists in discriminating between the products of WIMP annihilation and "background" cosmic ray (CR) particles. The smallest background arises when considering antiprotons and positrons, secondary products of interactions of CR particles with interstellar matter, and thus these provide the best opportunity to search for dark matter signatures [3–6]. A search for a distinct signature in  $\gamma$ -rays from the Galactic halo has also been proposed [7].

Though the microphysics is quite well understood and many groups make sophisticated calculations of the spectra of annihilation products for numerous WIMP candidates which include many decay chains [4,8], there are still uncertainties in the macrophysics which could change the estimated fluxes of WIMP annihilation products by 1–2 orders of magnitude, making predictions for their detection difficult. In the case of antiprotons the strongest evidence would be detection of low energy particles [3,4] (below  $\sim 1$  GeV in the interstellar space) but the solar wind and magnetic field sweep low energy particles away from the heliosphere, the effect known as solar modulation. In the case of  $\gamma$ -rays, a weak signal would compete with the flux of Galactic halo  $\gamma$ -rays, the uncertain background of extragalactic photons, and a contribution from unresolved sources.

The most promising is perhaps the positron signal since it can appear at high energies where the solar modulation is negligible, but its strength depends on many details of propagation in the Galaxy. The "leaky box" model is often used [5,6], a simplified approach which may not be applicable in the case of positrons. The most accurate propagation model applied so far, the diffusion model [8], is analytical and thus is subject to certain simplifications, e.g. the positron source function is treated as being dependent only on the radial cylindrical coordinate  $R$ , the assumption of spatially uniform interstellar radiation and magnetic fields, and some other minor details. On the other hand, progress in CR positron measurements is anticipated since several missions operating or under construction are capable of measuring positron fluxes up to 100 GeV (e.g. gas-RICH/CAPRICE and PAMELA experiments [9]). Therefore, more accurate calculation of the positron propagation is desirable.

We have developed a numerical method and corresponding computer code (GALPROP)\* for the calculation of Galactic CR propagation in 3D [10]. The rationale for our approach was given previously [10–15]. Briefly, the idea is to develop a model which simultaneously reproduces observational data of many kinds related to cosmic-ray origin and propagation: directly via measurements of nuclei, antiprotons, electrons, and positrons, indirectly via  $\gamma$ -rays and synchrotron radiation. These data provide many independent constraints on any model and our approach is able to take advantage of this since it aims to be consistent with many types of observation.

The code is sufficiently general that new physical effects can be introduced as required. Its capability includes primary and secondary nucleons, primary and secondary electrons,

---

\*Our model including software and datasets is available at <http://www.gamma.mpe-garching.mpg.de/~aws/aws.html>

secondary positrons and antiprotons, as well as  $\gamma$ -rays and synchrotron radiation. The basic spatial propagation mechanisms are diffusion and convection, while in momentum space energy loss and diffusive reacceleration are treated. Fragmentation, secondary particle production, and energy losses are computed using realistic distributions for the interstellar gas and radiation fields. We aim for a “standard model” which can be improved with new astrophysical input and additional observational constraints.

In this paper we use our model for calculation of positron propagation in different models of the dark matter halo distribution. We compare our predictions with evaluated cosmic ray positron spectra (“background”) for the “conventional” CR nucleon spectrum which matches the local measurements, and for a modified spectrum which respects the limits imposed by measurements of diffuse Galactic  $\gamma$ -rays, antiprotons, and positrons. To be specific we will further discuss neutralino dark matter, although our results can be easily adopted for any other particle dark matter candidate.

## II. BASIC FEATURES OF THE GALPROP MODELS

The GALPROP models have been described in full detail elsewhere [10]; here we just summarize briefly their basic features.

The models are three dimensional with cylindrical symmetry in the Galaxy, and the basic coordinates are  $(R, z, p)$  where  $R$  is Galactocentric radius,  $z$  is the distance from the Galactic plane and  $p$  is the total particle momentum. In the models the propagation region is bounded by  $R = R_h$ ,  $z = \pm z_h$  beyond which free escape is assumed.

The propagation equation we use for all CR species is written in the form:

$$\frac{\partial \psi}{\partial t} = q(\vec{r}, p) + \vec{\nabla} \cdot (D_{xx} \vec{\nabla} \psi - \vec{V} \psi) + \frac{\partial}{\partial p} p^2 D_{pp} \frac{\partial}{\partial p} \frac{1}{p^2} \psi - \frac{\partial}{\partial p} \left[ \dot{p} \psi - \frac{p}{3} (\vec{\nabla} \cdot \vec{V}) \psi \right] - \frac{1}{\tau_f} \psi - \frac{1}{\tau_r} \psi, \quad (1)$$

where  $\psi = \psi(\vec{r}, p, t)$  is the density per unit of total particle momentum,  $\psi(p) dp = 4\pi p^2 f(\vec{p})$  in terms of phase-space density  $f(\vec{p})$ ,  $q(\vec{r}, p)$  is the source term,  $D_{xx}$  is the spatial diffusion coefficient,  $\vec{V}$  is the convection velocity, reacceleration is described as diffusion in momentum space and is determined by the coefficient  $D_{pp}$ ,  $\dot{p} \equiv dp/dt$  is the momentum loss rate,  $\tau_f$  is the time scale for fragmentation, and  $\tau_r$  is the time scale for the radioactive decay.

An assumption is free escape of particles at the halo boundaries. Under certain simplifications it translates into the requirement that the number density of particles at the boundaries is zero:

$$\psi(R_h, z, p) = \psi(R, \pm z_h, p) = 0. \quad (2)$$

This is an approximation, but since the number density of particles there is presumably small, it is reasonable to assume

that this should not affect much the particle distribution in the Galaxy.

The numerical solution of the transport equation (1)–(2) is based on a Crank-Nicholson [16] implicit second-order scheme. Since we have a 3-dimensional  $(R, z, p)$  problem we use “operator splitting” to handle the implicit solution. We apply the implicit updating scheme alternately for the operator in each dimension in turn, keeping the other two coordinates fixed. A check for convergence is performed by computing the timescale  $\psi/(\partial\psi/\partial t)$  from eq. (1) and requiring that this be large compared to all diffusive and energy loss timescales. The details of our method are fully explained in [10].

For a given  $z_h$  the diffusion coefficient as a function of momentum and the reacceleration parameters is determined by CR Boron-to-Carbon (B/C) ratio. Reacceleration provides a natural mechanism to reproduce the B/C ratio without an ad-hoc form for the diffusion coefficient. The spatial diffusion coefficient is taken as  $\beta D_0 (\rho/\rho_0)^\delta$ . Our reacceleration treatment assumes a Kolmogorov spectrum with  $\delta = 1/3$ . For the case of reacceleration the momentum-space diffusion coefficient  $D_{pp}$  is related to the spatial coefficient  $D_{xx}$  [17]. The injection spectrum of nucleons is assumed to be a power law in momentum,  $dq(p)/dp \propto p^{-\gamma}$  for the injected particle density, if necessary with a break.

The total magnetic field is assumed to have the form

$$B_{tot} = B_0 e^{-(R-R_\odot)/R_B - |z|/z_B}. \quad (3)$$

The values of the parameters  $(B_0, R_B, z_B)$  are adjusted to match the 408 MHz synchrotron longitude and latitude distributions. The interstellar hydrogen distribution uses HI and CO surveys and information on the ionized component; the Helium fraction of the gas is taken as 0.11 by number. Energy losses for electrons by ionization, Coulomb interactions, bremsstrahlung, inverse Compton, and synchrotron are included, and for nucleons by ionization and Coulomb interactions. The distribution of cosmic-ray sources is chosen to reproduce the cosmic-ray distribution determined by analysis of EGRET  $\gamma$ -ray data [18] and was described in Ref. [10].

Positron production is computed as described in Ref. [11]; this includes a critical reevaluation of the secondary decay calculations.

Gas related  $\gamma$ -ray intensities are computed from the emissivities as a function of  $(R, z, E_\gamma)$  using the column densities of HI and H<sub>2</sub> for Galactocentric annuli based on 21-cm and CO surveys [18]. The interstellar radiation field (ISRF), which is used for calculation of the inverse Compton (IC) emission and electron energy losses, is calculated based on stellar population models and COBE results, plus the cosmic microwave background. Our results for diffuse continuum  $\gamma$ -rays, synchrotron radiation, and a new evaluation of the ISRF are given in Ref. [12].

An overview of our results is presented in Ref. [13] and full results for protons, Helium, positrons, and electrons in Ref. [11]. The evaluation of the B/C and  $^{10}\text{Be}/^9\text{Be}$  ratios, evaluation of diffusion/convection and reacceleration models, and full details of the numerical method are given in Ref. [10]. Antiprotons have been evaluated in the context of the “hard interstellar nucleon spectrum” hypothesis in Ref. [14].

TABLE I. Parameters of the dark matter profiles [19].

Model	$\rho_0$ , $\text{GeV cm}^{-3}$	$r_c$ , kpc
“isothermal”	0.43	2.8
Evans	0.51	7.0
alternative	0.38	0.9

### III. GREEN’S FUNCTIONS

To make a prediction of the positron flux at the solar position, one needs to know the source function  $f(\epsilon)$  which describes the spectrum of positrons from neutralino annihilation, and the Green’s function  $G(E, \epsilon)$  for their propagation in the Galaxy. Then the positron flux is a convolution

$$\frac{dF}{dE} = \langle \sigma v \rangle \frac{\rho_0^2}{m_\chi^2} \int d\epsilon G(E, \epsilon) \sum_i B_i f_i(\epsilon) \quad [\text{cm}^{-2} \text{s}^{-1} \text{sr}^{-1} \text{GeV}^{-1}], \quad (4)$$

where  $\langle \sigma v \rangle$  is the thermally averaged annihilation cross section,  $\rho_0$  is the local dark matter mass density,  $m_\chi$  is the neutralino mass,  $B_i$  is the branching ratio into a given final state  $i$ . The Green’s function thus includes all details of the dark matter mass distribution and Galactic structure (diffusion coefficient, spatially and energy dependent energy losses etc.).

Following Kamionkowski and Kinkhabwala [19] we consider three different dark matter mass density profiles which match the Galactic rotation curve. The canonical “isothermal” sphere profile,

$$\rho(r) = \rho_0 \frac{r_c^2 + R_\odot^2}{r^2 + r^2}, \quad (5)$$

where  $r_c$  is the core radius,  $R_\odot = 8.5$  kpc is the solar distance from the Galactic center, and  $r^2 = R^2 + z^2$  is the spherical radial coordinate. The spherical Evans model,

$$\rho(r) = \rho_0 \frac{(r_c^2 + R_\odot^2)^2}{3r_c^2 + R_\odot^2} \frac{3r_c^2 + r^2}{(r_c^2 + r^2)^2}, \quad (6)$$

and an alternative form which also might be empirically acceptable,

$$\rho(r) = \rho_0 \frac{(r_c + R_\odot)^2}{(r_c + r)^2}. \quad (7)$$

Note that  $\rho_0$  and  $r_c$  for each model must be fitted to the rotation curve, and therefore they are different for each model (see Table I). These profiles are plotted in Fig. 1.

For each given model we calculate the Green’s function  $G(E, \epsilon)$  defined in Eq. (4), which gives the positron flux at the solar position corresponding to the positron source function in the form of a Dirac  $\delta$ -function in energy. The positron propagation is calculated in a model which was tuned to match many available astrophysical data [10,12]. Since the halo size in the range  $z_h = 4 - 10$  kpc is favored by our analyses of B/C and  $^{10}\text{Be}/^9\text{Be}$  ratios and diffuse Galactic  $\gamma$ -ray emission

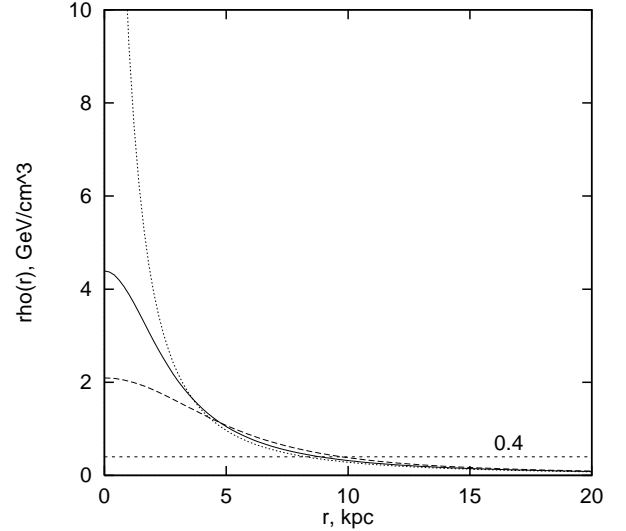


FIG. 1. The radial profiles of the spherical halo models: the canonical isothermal model (solid line), Evans model (long dashes), alternative model (dots), and uniform distribution ( $\rho = 0.4 \text{ GeV cm}^{-3}$ , short dashes).

[10,12], we consider two cases  $z_h = 4$  and 10 kpc which provide us with an idea of the possible limits. The preferred neutralino mass range following from accelerator and astrophysical constraints is  $50 \text{ GeV} < m_\chi < 600 \text{ GeV}$  [20], and we consider positron energies  $\epsilon \leq 824 \text{ GeV}$  which cover this range.

For the case of a uniform dark matter mass distribution  $\rho(r) = \langle \rho \rangle = \text{const}$  we compare our results with simple analytical Green’s functions for the leaky-box model for two cases, where the positron containment time is a constant parameter,  $\tau = \tau_0$ ,

$$G_1(E, \epsilon) = \frac{c}{4\pi\xi} \frac{1}{E^2} \exp\left(\frac{\epsilon^{-1} - E^{-1}}{\tau_0\xi}\right) \theta(\epsilon - E), \quad (8)$$

and when it varies with energy,  $\tau(\epsilon) = \eta/\epsilon$ ,

$$G_2(E, \epsilon) = \frac{c}{4\pi\xi} \frac{1}{\epsilon^2} \left[\frac{E}{\epsilon}\right]^{\frac{1}{\xi\eta}-2} \theta(\epsilon - E), \quad (9)$$

where  $c$  is the speed of light,  $\eta$  is a constant,  $\xi$  is the energy loss constant  $d\epsilon/dt = \xi\epsilon^2$ , and  $\theta(x)$  is the Heaviside step function.

Fig. 2 shows functions  $E^2G(E, \epsilon)$  calculated in our model for Galactic halo sizes  $z_h = 4$  and 10 kpc compared to the leaky-box functions  $G_{1,2}(E, \epsilon)$ . For this comparison we adopted the following parameters [6]:  $G_1$ :  $\xi = 1.11 \times 10^{-9} \text{ yr}^{-1} \text{ GeV}^{-1}$ ,  $\tau_0 = 10^7 \text{ yr}$ ;  $G_2$ :  $\xi = 1.52 \times 10^{-9} \text{ yr}^{-1} \text{ GeV}^{-1}$ ,  $\eta = 2 \times 10^8 \text{ yr GeV}$ . It is clear that the leaky-box model does not work here, moreover a reasonable fit to our  $G$ -functions is impossible for any combination of  $\xi$  and  $\tau_0$  (or  $\eta$ ). The difference in the normalization at maximum ( $E = \epsilon$ ) is mainly connected with our accurate calculation of the ISRF which is responsible for the energy losses.

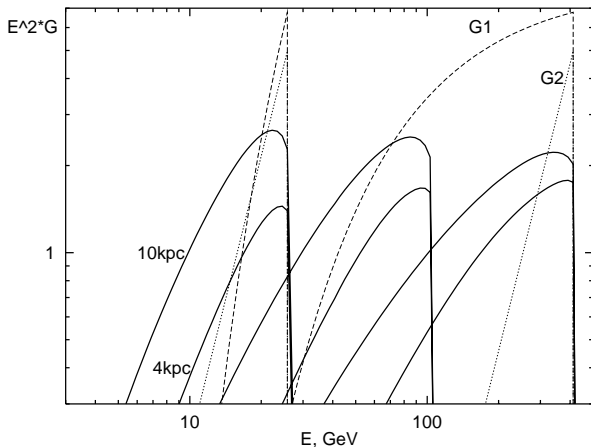


FIG. 2. Calculated  $G$ -functions for the uniform dark matter distribution,  $z_h = 4$  kpc and 10 kpc, for  $\epsilon = 25.76, 103.0, 412.1$  GeV (solid lines). The leaky-box functions  $G_1$  and  $G_2$  are shown by dashed and dotted lines respectively. The units of the abscissa are  $10^{25}$  GeV cm sr $^{-1}$ .

Fig. 3 shows our calculated  $G$ -functions for different models of the dark matter distribution: “isothermal”, Evans, and alternative. The curves are shown for two halo sizes  $z_h = 4$  and 10 kpc and several energies  $\epsilon = 1.03, 2.06, 5.15, 10.3, 25.8, 51.5, 103.0, 206.1, 412.1, 824.3$  GeV. At high energies, increasing positron energy losses due to the IC scattering compete with the increasing diffusion coefficient, while at low energies increasing energy losses due to the Coulomb scattering and ionization [10] compete with energy gain due to reacceleration. The first effect leads to a smaller sensitivity to the halo size at high energies. The second one becomes visible below  $\sim 5$  GeV and is responsible for the appearance of accelerated particles with  $E > \epsilon$ .

It is interesting to note that for a given initial positron energy all three dark matter distributions provide very similar values for the maximum of the  $G$ -function (on the  $E^2 G(E, \epsilon)$  scale), while their low-energy tails are different. This is a natural consequence of the large positron energy losses. Positrons contributing to the maximum of the  $G$ -function originate in the solar neighbourhood, where all models give the same dark matter mass density [see eq. (4) for the definition of the  $G$ -function]. The central mass density in these models is very different (Fig. 1), and therefore the shape of the tail is also different since it is produced by positrons originating in distant regions. As compared to the isothermal model, the Evans model produces sharper tails, while the alternative model gives more positrons in the low-energy tail. At intermediate energies ( $\sim 10$  GeV) where the energy losses are minimal, the difference between  $z_h = 4$  and 10 kpc is maximal. Also at these energies positrons from dark matter particle annihilations in the Galactic center can contribute to the predicted flux. This is clearly seen in the case of the alternative model with its very large central mass density (Fig. 3c,  $z_h = 10$  kpc).

To provide the Green’s function for an arbitrary positron energy, which is necessary for prediction of positron fluxes in the case of continuum positron source functions (as will be

required if one considers secondary, tertiary etc. decay products), we made a fit to our numerical results. Since a reasonable fit using the leaky-box Green’s functions is impossible we have chosen the function

$$G(E, \epsilon) = \frac{10^{25}}{E^2} \left\{ 10^{a \log^2 E + b \log E + c} \theta(\epsilon - E) + 10^{w \log^2 E + x \log E + y} \theta(E - \epsilon) \right\} \quad [\text{cm sr}^{-1} \text{ GeV}^{-1}], \quad (10)$$

which allows us to fit our numerical functions with accuracy better than 10% over a decade in magnitude (on the  $E^2 G(E, \epsilon)$  scale). Here the first term fits the low energy tail, the second term fits the right-hand-side part of the  $G$ -functions and represents the effect of reacceleration,  $E$  is in GeV, and  $a(\epsilon), b(\epsilon), c(\epsilon), w(\epsilon), x(\epsilon), y(\epsilon)$  are the fitting parameters. Though a better fit is possible by using more complicated functions, we try to minimize the number of fitting parameters while still providing reasonable accuracy. Besides, the accuracy of our propagation model is not better than 10%, being limited by the accuracy of the astrophysical data input. The numerical values of the fitting parameters are given in Tables II–III for the three models discussed. At intermediate energies the parameters can be interpolated. The cubic spline (or square spline for  $w, x, y$ ) provides  $\sim 10\%$  accuracy for the  $G$ -functions when interpolating on the logarithmic energy scale.

## IV. POSITRON FLUXES

### A. Positrons from the dark-matter particles annihilation

When neutralinos annihilate in the Galactic halo they produce quarks, gluons, leptons, and other particles which via hadronization and/or decays give rise to secondary positrons. One can expect to get both monoenergetic positrons (energy  $m_\chi$ ) from direct annihilation into  $e^+e^-$  and continuum positrons from the other annihilation channels. In general, the direct  $e^+e^-$  annihilation channel is severely suppressed with a branching ratio of order  $10^{-5}$  [5], though some classes of models allow a larger branching ratio to be obtained. Also in some cases, e.g. if annihilation occurs near a pole in the cross section,  $\langle \sigma v \rangle$  can be quite large [21] which can compensate for a small branching ratio. The (quasi-) monoenergetic positron line, if it is strong enough, is easier to identify. In contrast, the hadronization and/or decay cascades lead to the appearance of “continuum” positrons with correspondingly degraded energy thus making worse the signal/background ratio.

For a neutralino heavier than  $W^\pm$  ( $Z^0$ ) boson, annihilation to  $W^\pm$ - or  $Z^0$ -boson pairs will be significant followed by the direct decay of  $W^+$ ’s and  $Z^0$ ’s to lepton pairs where the direct positron channel accounts for 11% and 3.4% of  $W^+$  and  $Z^0$  decays, respectively. In the case where the neutralino is a pure Higgsino state, the annihilation cross section to  $W^\pm$ - or  $Z^0$ -boson pair increases rapidly above the threshold and reaches a maximum of  $\langle \sigma v \rangle \approx 3 \times 10^{-25}$  cm $^3$  s $^{-1}$  (for  $W^+W^-$ ) and  $\approx 2 \times 10^{-25}$  cm $^3$  s $^{-1}$  (for  $Z^0Z^0$ ) at about 110 GeV and

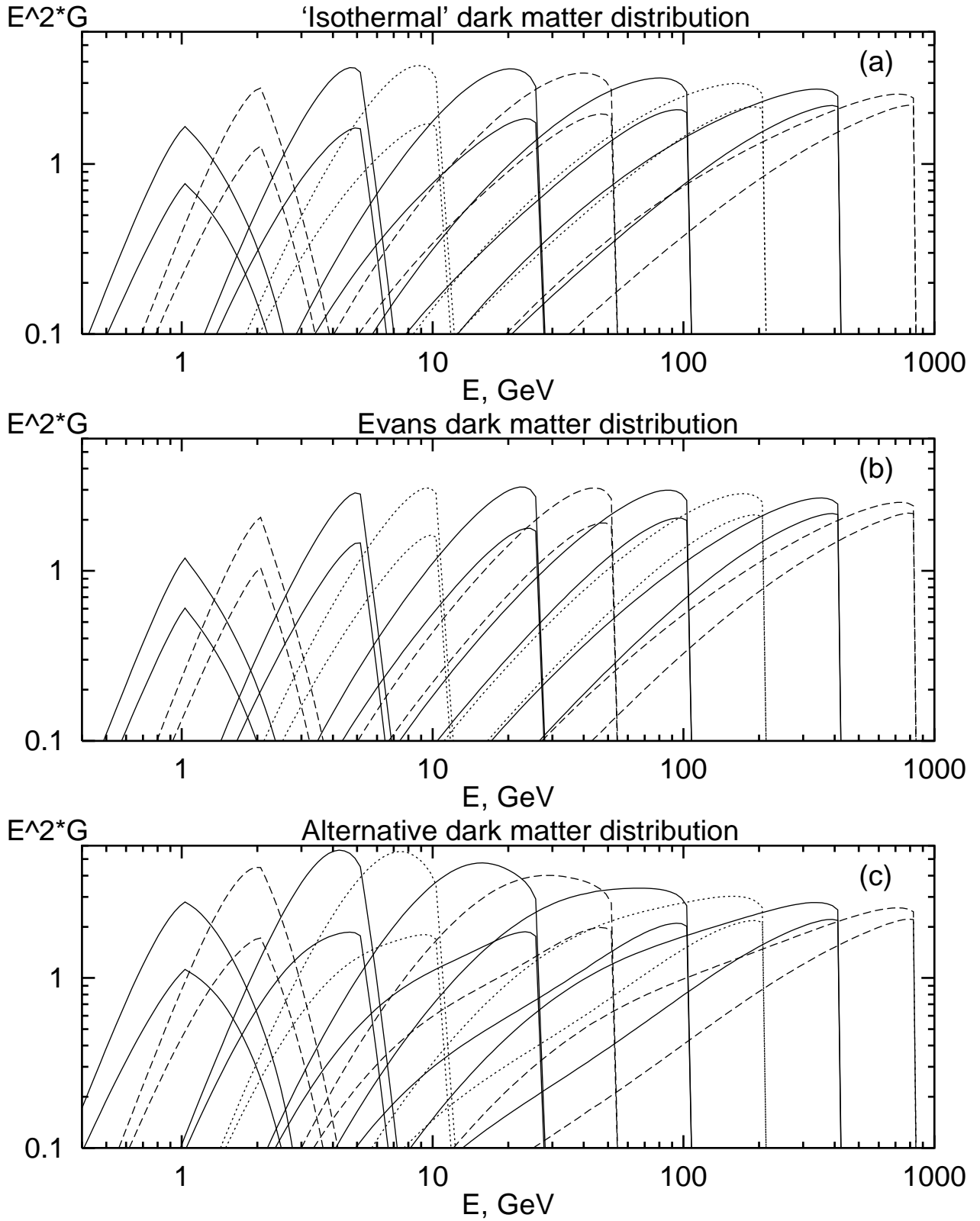


FIG. 3. Calculated  $G$ -functions for different models of the dark matter distribution: (a) “isothermal”, (b) Evans, (c) alternative. Upper curves  $z_h = 10$  kpc, lower curves  $z_h = 4$  kpc,  $\epsilon = 1.03, 2.06, 5.15, 10.3, 25.8, 51.5, 103.0, 206.1, 412.1, 824.3$  GeV. The units of the abscissa are  $10^{25}$  GeV cm sr $^{-1}$ .

TABLE II. Fitting parameters of the Green's functions.

$\epsilon$ , GeV	"isothermal" model			Evans model			alternative model		
	$a$	$b$	$c$	$a$	$b$	$c$	$a$	$b$	$c$
$z_h = 4$ kpc									
1.03	-1.9732	2.3448	-0.1340	-1.9937	2.6865	-0.2421	-2.0146	1.8984	0.0364
2.06	-2.4853	3.2517	-0.6564	-2.2043	3.5919	-0.8762	-2.9275	2.7980	-0.3409
5.15	-2.6365	4.4743	-1.6189	-2.4577	4.7878	-1.9748	-3.0137	4.1174	-1.1397
10.30	-1.9555	4.4101	-2.2099	-1.9686	4.8817	-2.6923	-2.0712	3.9274	-1.6167
25.76	-1.1684	3.7535	-2.6853	-1.3763	4.5614	-3.4205	-0.9412	2.7981	-1.8075
51.52	-0.8469	3.3985	-3.0180	-1.1035	4.3731	-3.9446	-0.4843	2.0882	-1.8434
103.00	-0.6979	3.3043	-3.4776	-0.9532	4.3484	-4.5560	-0.2718	1.6991	-1.9641
206.10	-0.6173	3.3187	-4.0118	-0.8078	4.1933	-5.0264	-0.2586	1.8175	-2.4451
412.10	-0.5337	3.2338	-4.4403	-0.6719	3.9382	-5.3478	-0.3292	2.2664	-3.2998
824.30	-0.4255	2.9458	-4.6095	-0.5078	3.4153	-5.2860	-0.3330	2.4540	-3.9563
$z_h = 10$ kpc									
1.03	-2.9531	2.2688	0.2037	-2.2651	2.7232	0.0540	-3.9088	1.6600	0.4355
2.06	-4.3610	4.1399	-0.4085	-3.3310	4.1276	-0.6391	-5.3710	4.0111	-0.0642
5.15	-4.6245	6.7914	-1.9188	-3.7297	6.2467	-2.0800	-5.8784	7.5056	-1.6622
10.30	-3.6318	7.1054	-2.9096	-3.0093	6.5384	-3.0367	-4.7439	8.2050	-2.8244
25.76	-2.3450	6.2626	-3.6392	-2.0541	5.9838	-3.8567	-2.8799	6.8568	-3.4165
51.52	-1.6556	5.3936	-3.8732	-1.5142	5.3295	-4.1955	-1.8345	5.3634	-3.3196
103.00	-1.1707	4.5572	-3.9405	-1.1606	4.8040	-4.4885	-1.1501	4.0735	-3.0763
206.10	-0.8276	3.8034	-3.9013	-0.8889	4.2660	-4.6500	-0.7058	3.0354	-2.7952
412.10	-0.5822	3.1489	-3.8069	-0.6680	3.6993	-4.6643	-0.4132	2.2082	-2.5103
824.30	-0.3984	2.5623	-3.6580	-0.4917	3.1504	-4.5846	-0.2256	1.5851	-2.2758

TABLE III. Fitting parameters of the Green's functions.

$\epsilon$ , GeV	"isothermal" model			Evans model			alternative model		
	$w$	$x$	$y$	$w$	$x$	$y$	$w$	$x$	$y$
$z_h = 4$ kpc									
1.03	-4.9292	-0.8786	-0.1115	-4.0224	-1.4477	-0.2053	-5.9792	-0.1569	0.0412
2.06	-7.2475	1.0942	0.4742	-6.5523	0.1919	0.6011	-8.1532	2.2559	0.3291
5.15	-8.9618	2.1785	3.1988	-8.0219	0.4044	3.9380	-9.3685	3.1591	2.7479
$z_h = 10$ kpc									
1.03	-4.3201	-1.1227	0.2324	-3.5986	-1.4890	0.0867	-5.3468	-0.6192	0.4554
2.06	-6.0920	0.2541	0.9683	-4.2529	-1.4473	1.1879	-8.0942	2.1474	0.7739
5.15	-6.5457	-1.1929	4.7067	-10.0800	3.5947	3.0000	-9.0223	3.1302	3.0000

120 GeV, respectively [6]. For unpolarized  $W^+$ -boson the decay is isotropic in the rest frame, which produces a uniform positron distribution in the laboratory system:

$$f(\epsilon) = \frac{1}{m_\chi \beta_W} \theta(\epsilon - \epsilon_-) \theta(\epsilon_+ - \epsilon) \quad (11)$$

where  $\beta_W$  is the  $W^+$ -boson speed in the laboratory system, and  $\epsilon_\pm = \frac{1}{2}m_\chi(1 \pm \beta_W)$ . Since the CR positron spectrum falls as  $\sim E^{-3.3}$  above several GeV [22], and the signal strength is proportional to  $\epsilon^{-2}m_\chi^{-3}$ , the signal/background ratio is maximal near  $m_\chi \sim m_W$ .

### B. Positron "background"

An important issue in interpretation of the positron measurements is evaluation of the "background", positrons arising

from CR particle interactions with interstellar matter. Though the parameters of the propagation and the Galactic halo size can be fixed in a self-consistent way using CR isotope ratios, the ambient CR proton spectrum on the Galactic scale remains quite uncertain.

The only possibility to trace the spectrum of nucleons on a large scale is to observe secondary products such as diffuse  $\gamma$ -rays, positrons, and antiprotons. The EGRET data show enhanced  $\gamma$ -ray emission above 1 GeV in comparison with calculations based on locally measured ("conventional") proton and electron spectra [23]. This can be interpreted as implying that the average spectra of particles in the Galaxy can differ from what we measure locally, due to details of Galactic structure and, in the case of electrons, large energy losses. A possible solution could be a hard interstellar proton spectrum [24], or an electron spectrum which is on average harder than that locally observed [25,26] due to the spatially inhomogeneous source distribution and energy losses.

The first possibility has been studied in detail in relation to antiprotons and positrons [12,14], showing that the resulting particle fluxes are too large. Taken together, the antiproton and positron data provide rather substantial evidence against the idea of explaining the  $>1$  GeV  $\gamma$ -ray excess with a hard nucleon spectrum.

The second possibility looks more plausible and detailed calculations [12,26] showed that the  $\gamma$ -ray excess could indeed be explained in terms of IC emission from a hard electron spectrum, but the fit to the EGRET spectral shape is still not very good. It can be further improved by allowing some freedom in the nucleon spectrum at low energies, which is possible since solar modulation affects direct measurements of nucleons below 20 GeV. Because of the hard electron spectrum the required modification to the nucleon spectrum is moderate; as expected the predictions for antiproton and positron fluxes are larger than in the “conventional” model but still within the allowed limits [12].

In order to show the effect of varying of the ambient proton spectrum, we compare our results with two models for the CR positron “background”. These are a “conventional” model (model C) which reproduces the local directly measured proton and Helium spectra above 10 GeV (where solar modulation is small), and a model with modified nucleon spectrum (model HEMN), which is flatter below 20 GeV and steeper above, and arises from our analysis of Galactic diffuse  $\gamma$ -ray emission. The “background” spectra are slightly dependent on the halo size. Since all secondary particles are produced in the Galactic plane, increasing the halo size results only in a small decrease of the flux at high energies due to larger energy losses. The propagation parameters for these models are given in Refs. [10,12], and the formalism for calculation of secondary positrons is described in Ref. [11].

### C. Calculations

We do not intend to make sophisticated calculations of positron spectra resulting from numerous decay chains such as best done by, e.g., Baltz and Edsjö [8] for many WIMP candidates. Instead, for illustration purposes, we simplify our analysis by treating the annihilation to  $W^\pm$  and  $Z^0$ -pairs. For  $m_\chi < m_W$  we consider only the direct annihilation to  $e^+e^-$  pairs. In the first case we use the cross sections for a pure Higgsino [6] and the production source function given by Eq. (11), in the latter case we take  $B \cdot \langle\sigma v\rangle = 3 \times 10^{-28} \text{ cm}^3 \text{ s}^{-1}$  and monoenergetic positrons. These parameters can be considered as optimistic, but possible [5,6]. To maximize the signal we further choose the Galactic halo size as 10 kpc.

Fig. 4 shows our predictions for the two CR positron “background” models together with HEAT data [22] and positrons from neutralino annihilation. It is seen that the predicted signal/background ratio has a maximum near  $m_\chi \sim m_W$ , while even in the “conventional” model the background is nearly equal to the signal at its maximum. It is however interesting to note that our calculations in this model show some excess in low energy ( $\leq 10$  GeV) positrons where the measurements

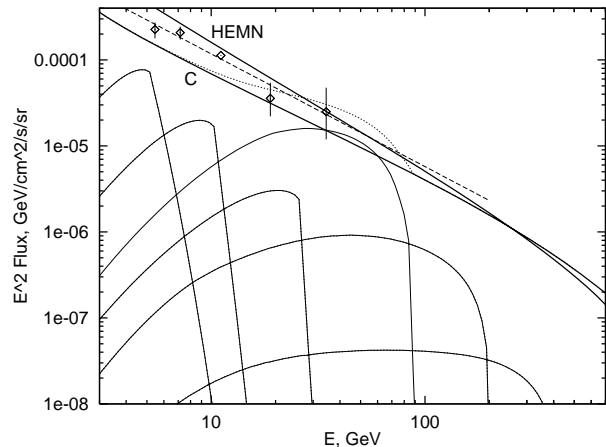


FIG. 4. Our predictions for two CR positron “background” models (C and HEMN: heavy solid lines), and positron signals from neutralino annihilation for  $m_\chi = 5.15, 10.3, 25.8, 103.0, 206.1, 412.1$  (thin solid lines): (a)  $z_h = 4$  kpc, (b)  $z_h = 10$  kpc. In the case of  $m_\chi = 103.0$  GeV, the signal plus background (model C) is shown by the dotted line. Data and the best fit to the data (dashes) are from Ref. [22] (HEAT collaboration).

are rather precise but the solar modulation is also essential. If this excess testifies to a corresponding excess in interstellar space and if the positron background correspond to our “conventional” calculations, it could be a hint for the presence of dark matter [8,27]. Our HEMN model fits the HEAT data better (no excess) and thus provides more background positrons. (This shows that in principle a good fit to positron data, which is consistent also with other measurements such as  $\gamma$ -rays and antiprotons is possible without any additional positron source.) Under such circumstances a significant detection of a weak signal would require favourable conditions and precise measurements. Though this our conclusion qualitatively agrees with that of Baltz and Edsjö [8] and several earlier papers, it is based on a more realistic model of particle propagation and thus reduces the scope for future speculations.

We should mention, however, a possibility which could increase the signal by orders of magnitude. Relatively small fluctuations in the dark matter density distribution will strongly increase the positron yield; this would be the case if the dark matter halo is clumpy [28]. But even if such a signal is detected, its correct interpretation will require reliable background calculations and thus emphasizes the necessity for further developments in modelling production and propagation of CR species in the Galaxy.

### V. CONCLUSION

We have made a calculation of propagation of positrons from dark-matter particle annihilation in the Galactic halo using our 3D model which aims to reproduce simultaneously observational data of many kinds related to cosmic-ray origin and propagation: directly via measurements of nuclei, antiprotons, electrons, and positrons, indirectly via  $\gamma$ -rays and

synchrotron radiation. We use this model for the calculation of positron propagation in different models of the dark matter halo distribution and present fits to our numerical propagation Green's functions.

We have shown that the Green's functions are not very sensitive to the dark matter distribution for the same local dark matter energy density. This is a natural consequence of the large positron energy losses. The differences in the central dark matter mass density lead to different shapes of the Green's function low-energy tail, since this involves positrons originating in distant regions. As compared to the isothermal model, the Evans model produces sharper tails, while alternative model gives more positrons in the low-energy tail.

We compare our predictions with the computed CR positron "background" for two models of the CR nucleon spectrum. We conclude that a significant detection of a dark matter signal requires favourable conditions and precise measurements unless the dark matter is clumpy which would produce a stronger signal. Though our result qualitatively agrees with that of previous authors, it is based on a more realistic model of particle propagation and thus provides a firmer basis for conclusions.

A correct interpretation of positron measurements requires reliable background calculations and thus emphasizes the necessity for further developments in modelling production and propagation of CR species in the Galaxy. The ambient proton spectrum is of primary importance; its study requires combined approach which allows to evaluate  $\gamma$ -ray, antiproton and other data simultaneously.

#### ACKNOWLEDGMENTS

The authors thank the anonymous referee for his valuable comments.

---

<sup>§</sup> Also at D. V. Skobel'syn Institute of Nuclear Physics, M. V. Lomonosov Moscow State University, 119 899 Moscow, Russia.

- [1] V. Trimble, *Ann. Rev. Astron. Astrophys.* **25**, 425 (1989); K. M. Ashman, *Proc. Astro. Soc. Pac.* **104**, 1109 (1992).
- [2] G. Jungman, M. Kamionkowski, and K. Griest, *Phys. Rep.* **267**, 195 (1996).
- [3] J. Silk and M. Srednicki, *Phys. Rev. Lett.* **53**, 624 (1984); S. Rudaz and F. Stecker, *Astrophys. J.* **325**, 16 (1988); F. Stecker and A. Tylka, *Astrophys. J.* **336**, L51 (1989); J. Ellis *et al.*, *Phys. Lett.* **214**, 403 (1989).
- [4] See e.g. G. Jungman and M. Kamionkowski, *Phys. Rev. D* **49**, 2316 (1994); P. Chardonnet, G. Mignola, P. Salati, and R. Taillet, *Phys. Lett.* **384**, 161 (1996); A. Bottino, F. Donato, N. Fornengo, and P. Salati, *Phys. Rev. D* **58**, 123503 (1998); L. Bergström, J. Edsjö, and P. Ullio, *astro-ph/9902012*; See also Ref. [2] and references therein.
- [5] A. J. Tylka, *Phys. Rev. Lett.* **63**, 840 (1989); M. S. Turner and F. Wilczek, *Phys. Rev. D* **42**, 1001 (1990).
- [6] M. Kamionkowski and M. S. Turner, *Phys. Rev. D* **43**, 1774 (1991).
- [7] See e.g. H.-U. Bengtsson *et al.*, *Nucl. Phys.* **346**, 129 (1990); S. Rudaz and F. Stecker, *Astrophys. J.* **368**, 406 (1991); V. Berezhinsky *et al.*, *Phys. Lett.* **325**, 136 (1994); P. Chardonnet *et al.*, *Astrophys. J.* **454**, 774 (1995); See also Ref. [2] and references therein.
- [8] E. A. Baltz and J. Edsjö, *Phys. Rev. D* **59**, 023511 (1998).
- [9] CAPRICE collaboration, G. Barbiellini *et al.*, in *Proc. 25th Int. Cosmic Ray Conf.* (Durban) **5**, 1 (1997); PAMELA collaboration, O. Adriani *et al.*, in *Proc. 25th Int. Cosmic Ray Conf.* (Durban) **5**, 49 (1997).
- [10] A. W. Strong and I. V. Moskalenko, *Astrophys. J.* **509**, 212 (1998).
- [11] I. V. Moskalenko and A. W. Strong, *Astrophys. J.* **493**, 694 (1998).
- [12] A. W. Strong, I. V. Moskalenko, and O. Reimer, *Astrophys. J.*, submitted (1999), *astro-ph/9811296*.
- [13] A. W. Strong and I. V. Moskalenko, in *Topics in Cosmic Ray Astrophysics*, ed. M. A. DuVernois (Nova Scientific, New York, 1999), in press, *astro-ph/9812260*; in *Proc. of the Workshop "LiBeB, Cosmic Rays and Gamma-Ray Line Astronomy"*, eds. R. Ramaty *et al.*, ASP Conf. Ser. 171 (Astron. Soc. Pacific, 1999), p. 154.
- [14] I. V. Moskalenko, A. W. Strong, and O. Reimer, *Astron. Astrophys.* **338**, L75 (1998).
- [15] I. V. Moskalenko and A. W. Strong, *Astrophys. J.*, submitted (1999), *astro-ph/9811284*.
- [16] W. H. Press *et al.*, *Numerical Recipes in FORTRAN*, 2nd Edition (Cambridge University Press, Cambridge, 1992)
- [17] V. S. Berezhinskii *et al.*, *Astrophysics of Cosmic Rays* (North Holland, Amsterdam, 1990); E. S. Seo and V. S. Ptuskin, *Astrophys. J.* **431**, 705 (1994).
- [18] A. W. Strong and J. R. Mattox, *Astron. Astrophys.* **308**, L21 (1996).
- [19] M. Kamionkowski and A. Kinkhabwala, *Phys. Rev. D* **57**, 3256 (1998).
- [20] J. Ellis, talk at the *Nobel Symposium* (Sweden), *astro-ph/9812211*.
- [21] K. Griest and D. Seckel, *Phys. Rev. D* **43**, 3191 (1991).
- [22] HEAT Collaboration, S. W. Barwick *et al.*, *Astrophys. J.* **498**, 779 (1998).
- [23] S. D. Hunter *et al.*, *Astrophys. J.* **481**, 205 (1997).
- [24] P. Gralewicz *et al.*, *Astron. Astrophys.* **318**, 925 (1997); M. Mori, *Astrophys. J.* **478**, 225 (1997).
- [25] T. A. Porter and R. J. Protheroe, *J. Phys. G: Nucl. Part. Phys.* **23**, 1765 (1997).
- [26] M. Pohl and J. A. Esposito, *Astrophys. J.* **507**, 327 (1998).
- [27] S. Coutu *et al.*, *Astropart. Phys.*, in press (1999), *astro-ph/9902162*.
- [28] See e.g. J. Silk and A. Stebbins, *Astrophys. J.* **411**, 439 (1993); L. Bergström, J. Edsjö, P. Gondolo, and P. Ullio, *Phys. Rev. D* **59**, 043506 (1999).